ACS APPLIED MATERIALS & INTERFACES

Letter

www.acsami.org

Lead-free Piezoelectrics Based on Potassium–Sodium Niobate with Giant d_{33}

Binyu Zhang,[†] Jiagang Wu,*[,†] Xiaojing Cheng,[†] Xiaopeng Wang,[†] Dingquan Xiao,[†] Jianguo Zhu,[†] Xiangjian Wang,[‡] and Xiaojie Lou[‡]

[†]Department of Materials Science, Sichuan University, 610064, P. R. China

[‡]Multi-disciplinary Materials Research Center, Frontier Institute of Science and Technology, Xi'an Jiaotong University, Xi'an 710054, P. R. China

ABSTRACT: High-performance lead-free piezoelectrics (d_{33} > 400 pC/N) based on $0.96(K_{0.5}Na_{0.5})_{0.95}Li_{0.05}Nb_{1-x}Sb_xO_3-0.04BaZrO_3$ with the rhombohedral-tetragonal (R–T) phase boundary have been designed and prepared. The R-T phase boundary lies the composition range of $0.04 \le x \le 0.07$, and the dielectric and piezoelectric properties of the ceramics with the compositions near the phase boundary are significantly enhanced. In addition, the ceramic with x = 0.07 has a giant d_{33} of ~425 pC/N, which is comparable to that (~416 pC/N) of textured KNN-based ceramics (Saito, Y.; Takao, H.; Tani, T.; Nonoyama, T.; Takatori, K.; Homma, T.; Nagaya, T.; Nakamura, M. *Nature* **2004**, *432*, 84). The underlying physical mechanisms for enhanced piezoelectric properties are addressed. We believe that the material system is the most promising lead-free piezoelectric candidates for the practical applications.

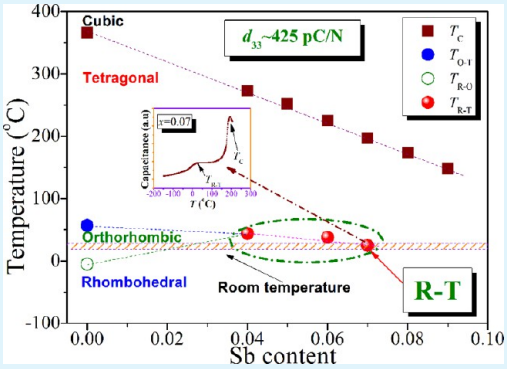

KEYWORDS: *lead-free piezoelectrics, giant d_{33}, potassium–sodium niobate, rombohedral-tetragonal phase boundary*

1. INTRODUCTION

$Pb(Zr,Ti)O_3$ (PZT) is always considered as one kind of high-performance piezoelectric materials, which are widely used in sensors, actuators, and other electronic devices.[1,2] However, these PZT-based ceramics with above 60 wt % Pb will be prohibited in the near future from many practical applications because of their toxicity during preparation and processing. Therefore, it is urgent to develop lead-free piezoelectrics to replace these lead-based ones. In 2004, Saito et al. reported on a giant piezoelectric constant (d_{33}) of ~416 pC/N in textured (K, Na, Li)(Nb, Ta, Sb)O_3 ceramics prepared by the reactive template grain growth method,[3] and then many researchers have made considerable efforts to develop the lead-free piezoelectrics based on $(K,Na)NbO_3$ (KNN) for obtaining the d_{33} comparable to PZT.[4−15]

Some attempts have been performed to enhance the d_{33} of the KNN-based ceramics.[3−34] In specific, several kinds of phase boundaries have been designed to improve the d_{33} of the KNN-based ceramics, and the d_{33} of 100−416 pC/N have been observed.[3−34] These reported d_{33} of the KNN-based ceramics, which were prepared by the conventional solid-state method, is often below 350 pC/N.[3−15,18−29] It is well-known that the rhombohedral–tetragonal (R-T) phase boundary, which is similar to the PZT, can greatly improve the piezoelectric properties of the KNN-based ceramics,[2,7,19,27] while their d_{33} is also always less than 370 pC/N. In addition, the d_{33} of the KNN-based ceramics depends on not only the phase boundary but also the composition. As a result, it may be a promising tool to further enhance the d_{33} of KNN based materials by constructing the R-T phase boundary using the optimum material system.

In this work, a giant d_{33} has been achieved by constructing a morphotropic phase boundary of the R-T phase coexistence in the $0.96(K_{0.5}Na_{0.5})_{0.95}Li_{0.05}Nb_{1-x}Sb_xO_3$ −0.04$BaZrO_3$ (KNLNS$_x$-BZ) system. In this system, adding Sb^{5+} can decrease T_{O-T} and increase T_{R-O} simultaneously.[18] Such a giant d_{33} of ~425 pC/N has been obtained by forming the R-T phase boundary, which exceeds those of the KNN ceramics with the complicated modifications using Li^+, Ta^{5+}, and Sb^{5+} dopants,[32,33] showing a promising candidate for the lead-free piezoelectric ceramics.

2. EXPERIMENTAL DETAILS

All the KNLNS$_x$-BZ samples with x = 0, 0.04, 0.05, 0.06, 0.07, 0.08, 0.09 were fabricated by the conventional solid-state reaction method, and the raw materials in this work were K_2CO_3, Na_2CO_3, Li_2CO_3, $BaCO_3$, ZrO_2, Nb_2O_5, and Sb_2O_3. These weighed powders were mixed with the alcohol for 24 h, then dried and calcined at 850 °C for 6 h. Calcined powders were mixed again and pressed into the pellets with 10 mm diameter and 1.0 mm thickness, and sintered at 1060−1130 °C for 3 h in air by the sealed sintering. It is well-known that the sealed sintering can depress the loss of the volatile elements during the sintering process.[35] In this work, the sealed sintering (i.e., double crucibles) has been conducted to prepare the KNLNS$_x$-BZ ceramics, and the schematic diagram has been given in Figure 1. The high

Received: June 29, 2013
Accepted: August 8, 2013
Published: August 12, 2013

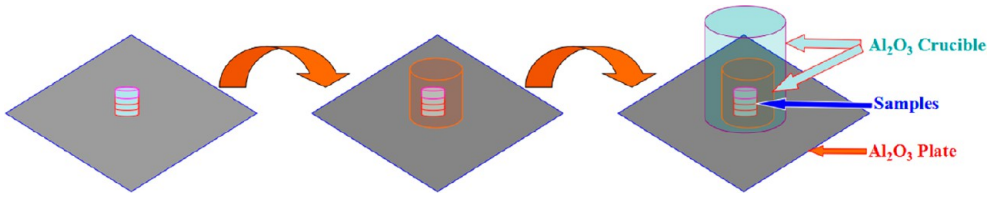

Figure 1. Schematic diagram of the sintering condition of KNNLS$_x$-BZ ceramics.

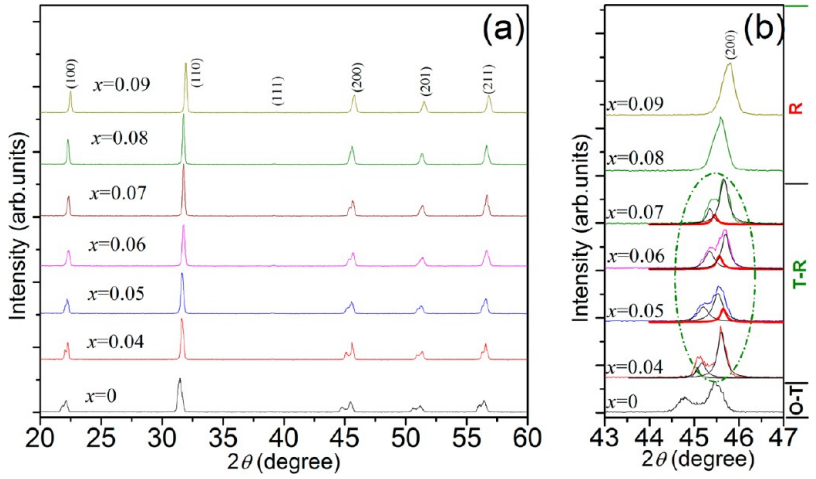

Figure 2. XRD patterns of KNLNS$_x$-BZ ceramics in the 2θ range of (a) 20−60° and (b) 43−47°.

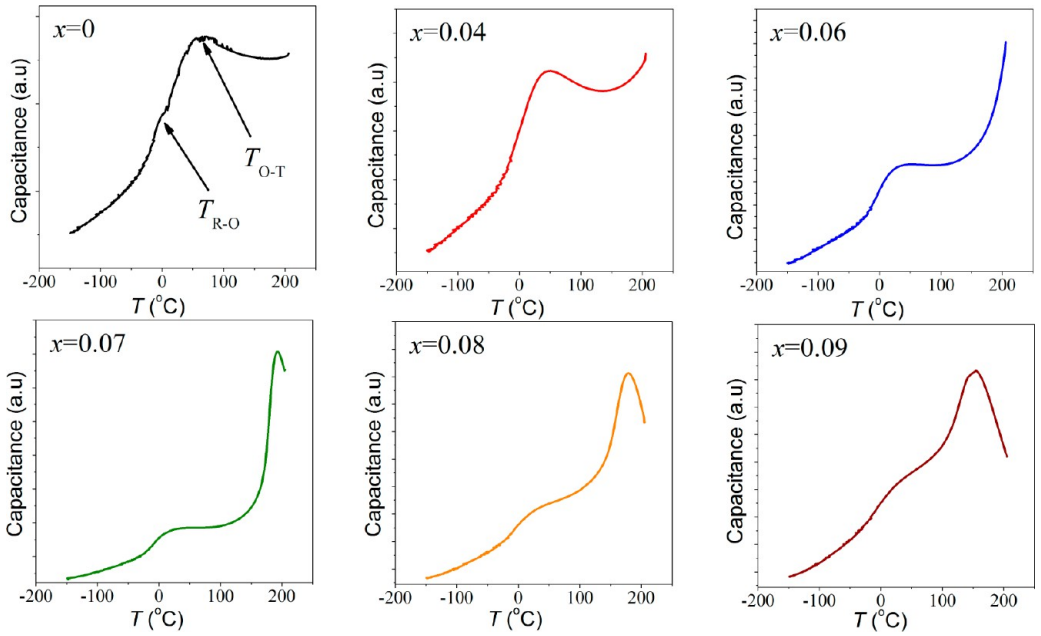

Figure 3. Temperature dependence of the capacitance of KNLNS$_x$-BZ ceramics in the measurement temperature from 200 °C to −150 °C.

volatilization of alkali metal oxides in KNN can be effectively suppressed at a high temperature during sintering by the method of double crucibles.[36] For this method, the outside and inside crucibles are made of Al_2O_3, and the KNLNS$_x$-BZ pellets are then sintered by covering with their powders. The silver paste was coated on the double surfaces and then fired at 700 °C for 30 min for the electrical measurements.

The electric poling of the samples was carried out in the range of 20−150 °C in a silicone oil bath by applying a dc field of 0.5−4.0 kV/mm for 20 min. The density of the sintered samples was measured by the Archimedes method. X-ray diffraction meter with a CuKa radiation (DX-2700, Dandong, China) has been used to identify the phase structure of the sintered cylindrical pellets. Their microstructure and element mapping were measured and recorded by a field-emission scanning electron microscope (FE-SEM) (JSM-7500, Japan). The capacitance and dissipation factors of the sintered samples were measured using an *LCR* analyzer (HP 4980, Agilent, U.S.A.) with a varied temperature between −150−200 °C and room temperature ~550 °C. The dielectric properties of the poled samples were evaluated at 1−100 kHz and the polarization versus electric field (*P*−*E*) hysteresis loops of the unpoled cylindrical pellets were measured at 10 Hz with a ferroelectric tester (Radiant Technologies, Inc. Albuquerque, NM, USA). The planar electromechanical coupling factor (k_p) was measured by a resonance-antiresonance method with

dx.doi.org/10.1021/am402548x | ACS Appl. Mater. Interfaces 2013, 5, 7718−7725

an impedance analyzer (Impedance Analyzer, PV70A, Beijing, China). The d_{33} was measured with a commercial Berlincourt-type d_{33} meter (ZJ-3A, China) for the poled samples.

3. RESULTS AND DISCUSSION

The room temperature XRD patterns of the KNLNS$_x$-BZ ceramics is shown in Figure 2(a). A pure perovskite phase has been observed in all the ceramics because of the lack of secondary phases, showing the formation of a stable solid solution. To detecting the phase evolution of the KNLNS$_x$-BZ ceramics as a function of Sb content, the expanded XRD patterns in 2θ = 43−47° are shown in Figure 2(b). We see that the ceramic with x = 0 shows orthorhombic−tetragonal (O-T) phase coexistence at room temperature.[34] As the Sb content further increases, the ceramic with $x \geq 0.08$ shows a rhombohedral phase.[19] Most interestingly, we find that the R-T phase coexistence can be formed in the ceramics with the composition range of $0.04 \leq x \leq 0.07$. For further characterizing the phase transition, the temperature -dependent dielectric behavior in the measurement temperature from 200 °C to −150 °C is shown in Figure 3. Recent studies have shown that adding Sb^{5+} can increase $T_{R\text{-}O}$ and lower $T_{O\text{-}T}$ of KNN.[18] In this work, the O-T phase boundary is shifted to the R-T phase coexistence as the Sb^{5+} content increases owing to the shrinkage of the O phase zone, resulting in the formation of the R-T phase boundary with the composition range of $0.04 \leq x \leq 0.07$. However, the R-T phase boundary of these ceramics becomes broadened gradually with increasing Sb^{5+} content ($x > 0.07$), showing the disappearance of the R-T phase boundary. It has been confirmed that the ceramics with $x \geq 0.08$ have a rhombohedral phase according to the XRD patterns.[19] As a result, the evolution of the phase structure has been further supported by the temperature-dependent dielectric properties measured in the temperature range of −150 to 200 °C.

Figure 4 shows the temperature-dependent dielectric constant (ε_r) of the KNLNS$_x$-BZ ceramics in the temperature

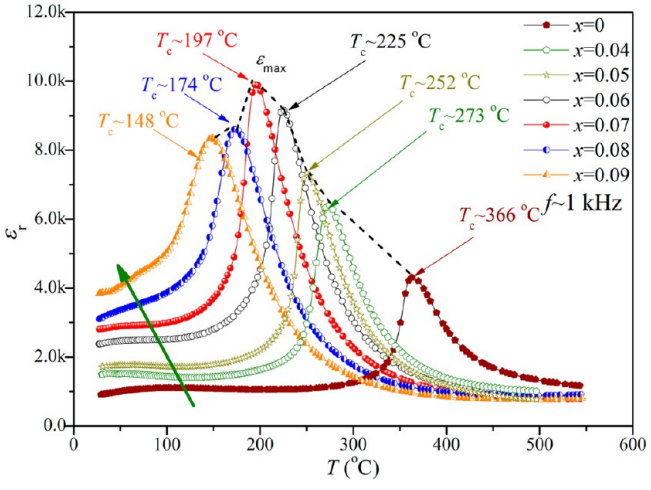

Figure 4. Temperature dependence of the dielectric constant of KNLNS$_x$-BZ ceramics in the temperature range of room temperature~550 °C.

range of room temperature~550 °C at 1 kHz. The ceramic with x = 0 undergoes two phase transitions above room temperature, that is, a tetragonal-cubic phase transition (T_C) at ~363 °C and an orthorhombic−tetragonal phase transition (T_{O-T}). Both T_C and T_{O-T} of these ceramics move to a lower temperature simultaneously, while $T_{R\text{-}O}$ shifts to a higher temperature with increasing Sb^{5+} content.[20,21] The T_C of all the ceramics is still above room temperature, further showing that the samples with $x \geq 0.08$ are a ferroelectric rhombohedral phase rather than a paraelectric cubic phase.[19,27] In addition, the ceramic with the R-T composition (x = 0.07) has a highest dielectric peak at T_C than those of the off phase boundary compositions, and such a phenomenon could be attributed to the formation of the R-T phase boundary.[19,32] Figure 5 plots the phase diagram of the

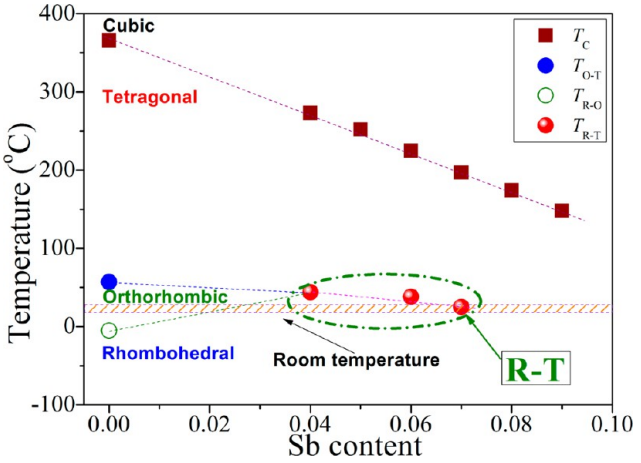

Figure 5. Phase diagram of KNLNS$_x$-BZ ceramics.

KNLNS$_x$-BZ ceramics according to the temperature -dependent dielectric behavior shown in Figures 3 and 4. The phase diagram shows that the addition of Sb^{5+} induces the shrinkage of the O phase. Finally, the R-T phase boundary has been formed in the ceramic with x = 0.07 at room temperature.

Figures 6a−d show the SEM patterns of the surface microstructure obtained from the KNLNS$_x$-BZ ceramics. The grain size first rises and then drops with increasing Sb content, showing a maximum value at x = 0.04. Similar phenomenon has been observed in the Sb^{5+}-modified KNN based ceramics.[37] As shown in Figure 6, the bimodal grain size distributions are shown in all the ceramics, more homogeneous and smaller grains have been involved into a pure KNLN-BZ ceramic, and the grain size becomes much larger for the ceramic with x = 0.04. However, the grains size refines as the Sb^{5+} content further increases (e.g., with x = 0.07). As a result, adding Sb^{5+} may refine the grain size of the KNLNS$_x$-BZ ceramics, which is similar to the function of Ba^{2+} in KNN-based ceramics[38] and the Sb-doped $(K_{0.5}Na_{0.5})_{0.945}Li_{0.055}Nb_{1-x}Sb_xO_3$ or $Bi_{0.5}(Na_{0.5}K_{0.5})_{0.5}TiO_3$ ceramics.[24,39] In addition, we can see from the inset of Figure 6c) that the cross section of the KNLNS$_x$-BZ ceramics with x = 0.07 shows a denser microstructure without observable pores. In this work, the distribution of chemical components in the sample with x = 0.07 is revealed using the energy dispersive X-ray analysis and the elemental distribution within bulk ceramics is profiled, as shown in Figure 7. From Figure 7, one can see that all the elements are homogeneously distributed in the ceramic. In addition, the variation of Sb elemental concentration of the KNLNS$_x$-BZ ceramics with x = 0.07 is recorded on a distance of about ~10 μm (see Figure 8). A continuous distribution of Sb ions is observed in the material, and the Sb concentration slightly fluctuates in the measurement range, further confirming that the Sb is homogeneously distributed in these materials. To character the influence of the density on the morphologies and electrical properties, the relative density of KNLNS$_x$-BZ ceramics has been

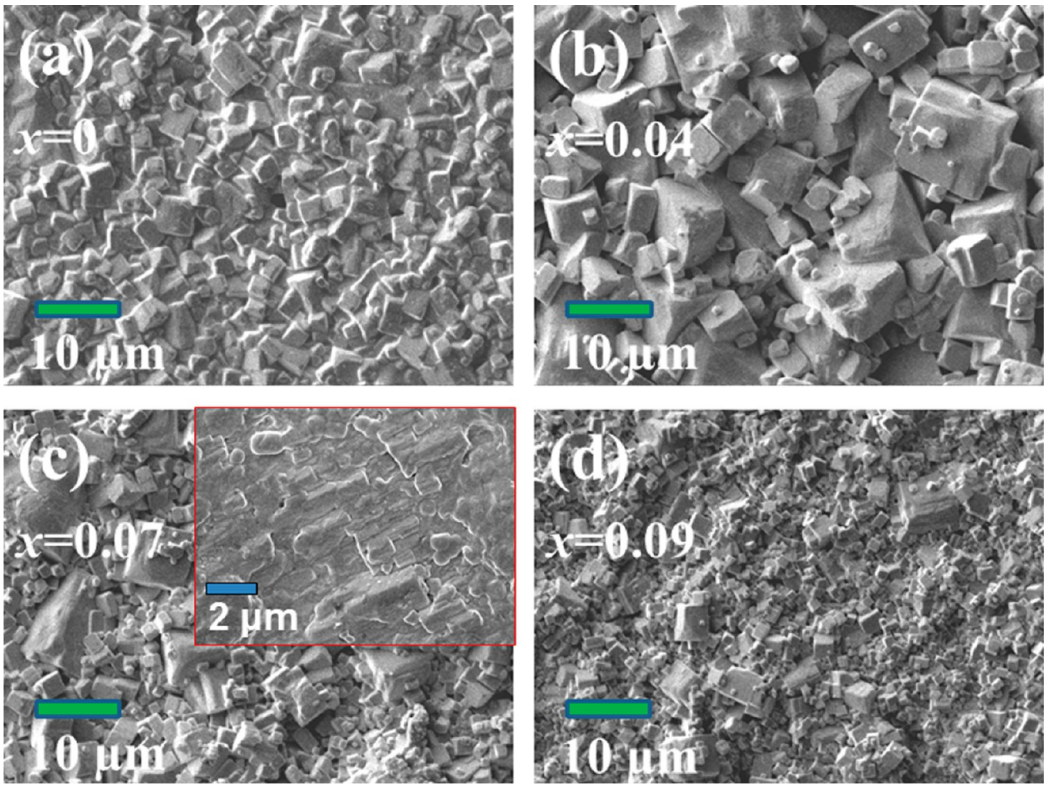

Figure 6. SEM patterns of KNLNS$_x$-BZ ceramics: (a) x = 0, (b) x = 0.04, (c) x = 0.07, and (d) x = 0.09; the inset in c is a polished cross-section after the thermal etching.

given in Figure 9. All the ceramics have a relatively higher density (>95%) as compared with reported KNN sintered under the atmospheric condition,[40] whereas the difference among them is also well-observed. The relative density of the samples gradually increases with rising Sb content, and the ceramics with $0.05 \leq x < 0.08$ possess a higher relative density (>97%), and then the density slightly decreases with further increasing Sb content ($x \geq 0.08$). The finement of the grains results in the decrease of pores at the junction.[41] Subsequently, the relationship between the density and the electrical properties is investigated, as shown later.

Figure 10 plots the dielectric constant (ε_r) and dielectric loss (tan δ) of the KNLNS$_x$-BZ ceramics, measured at 1, 10, and 100 kHz and room temperature. The dielectric behavior exhibits a similar trend with different frequencies. As shown in Figure 10, the ε_r quickly rises and then slightly fluctuates with increasing x content, and the increase in ε_r could be attributed to the addition of Sb^{5+}.[22−24] A maximum ε_m has been observed in the ceramic with x = 0.07, where the ε_m is defined as the maximum dielectric constant located at T_C. It was reported that the material located at the morphotropic phase boundary zone has a larger ε_m.[19,29] As a result, such a phenomenon further confirms the involvement of the phase boundary with the composition of x = 0.04. However, the tan δ first drops and gradually rises with increasing Sb^{5+} content. In this work, the composition dependence of tan δ well matches the change of the density [Figure 9], that is, a dense microstructure results in a low tan δ. As a result, the ceramic with x = 0.07 has an enhanced dielectric behavior of ε_r∼3157 and tan δ∼3.2%. In this work, the ε_r of ∼3157 is much larger than those of the KNN-based ceramics,[3,5,25−34] and is also larger than or comparable to those of the PZT-based ceramics.[1,2] Detailed parameters for the electrical properties of the KNLNS$_x$-BZ ceramics have been given in Table 1.

Figure 11a shows the P-E loops of the KNLNS$_x$-BZ ceramics as a function of Sb^{5+} content, measured at f = 10 Hz and room temperature. All the samples have well-defined P−E hysteresis loops because of a low leakage current density induced by the dense microstructure. It is observed from Figure 11a that the ferroelectric properties are degraded with the addition of Sb^{5+}, which is similar to those of the Sb^{5+} -modified KNN-based materials.[28,29] To accurately evaluate the effect of Sb^{5+} content on the ferroelectric properties, the P_r and E_c as a function of Sb^{5+} content is shown in Figure 11b. The P_r decreases gradually, and the E_c almost drops linearly.[28,29] It is well-known that adding Sb results in the decrease of the ferroelectric properties in KNN-based ceramics.[28,42−44] In addition, some experimental results have shown the grain size has a close relationship with the ferroelectric properties of KNN ceramics containing Sb,[18] that is, the ferroelectric properties are believed to degrade with the decrease of the grain size.[18,45,46] Some theories have shown that the spontaneous polarization of a ferroelectric material is depressed when the grain size decreases.[47] Comparing Figure 6 with Figure 11, a large grain size is well-observed for the ceramics with $x \leq 0.04$, resulting in a saturated P−E loop. However, the grain size gradually decreases with increasing Sb content ($x > 0.04$), degrading the ferroelectric properties. As a result, the grain size strongly affects the ferroelectric properties of KNLNS$_x$-BZ ceramics.

Figure 12 plots the d_{33} and k_p of the KNLNS$_x$-BZ ceramics with different Sb^{5+} content, measured at room temperature. The d_{33} of the KNLNS$_x$-BZ ceramics increases quickly and drops dramatically with increasing Sb^{5+} content, getting a maximum value of ∼425 pC/N at x = 0.07. An enhanced k_p is also

dx.doi.org/10.1021/am402548x | ACS Appl. Mater. Interfaces 2013, 5, 7718−7725

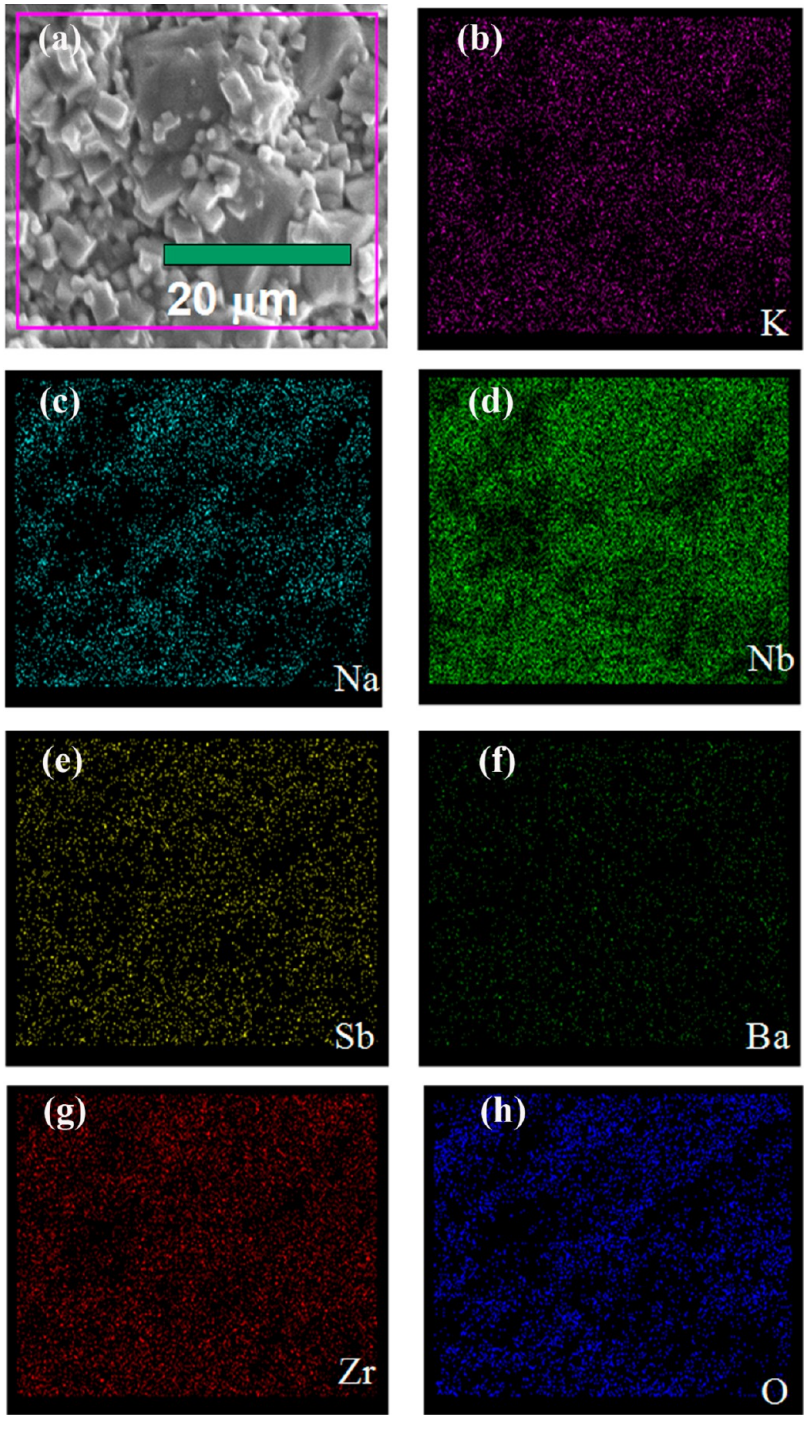

Figure 7. Elemental mapping of of KNLNS$_x$-BZ ceramics with x = 0.07.

Table 1. Dielectric, Ferroelectric, and Piezoelectric Properties of KNLNS$_x$-BZ Ceramics

composition	d_{33} pC/N	k_p	Q_m	P_r (μC/cm^2)	E_c (kV/cm)	ε_r 10 kHz	ε_{max} 1 kHz	tan δ 10 kHz	T_C (°C)
x = 0	174	0.32	70	22.2	15.2	810	4342	0.077	366
x = 0.04	223	0.38	59	21.8	12.8	1498	6403	0.064	273
x = 0.05	320	0.48	54	20.9	12.2	1715	7369	0.030	252
x = 0.06	370	0.51	47	19.0	10.8	2376	9172	0.033	225
x = 0.07	425	0.50	42	15.8	9.9	3157	9886	0.032	197
x = 0.08	320	0.37	55	13.2	8.9	3212	8587	0.038	174
x = 0.09	159	0.22	61	9.7	7.1	3407	8351	0.047	148

observed in the R-T phase boundary zone. As a result, the ceramic with x = 0.07 exhibits an enhanced piezoelectric behavior of $d_{33} \approx 425$ pC/N and $k_p \approx 50\%$. In this work, the d_{33} is larger than those reported results of KNN-based ceramics

dx.doi.org/10.1021/am402548x | ACS Appl. Mater. Interfaces 2013, 5, 7718−7725

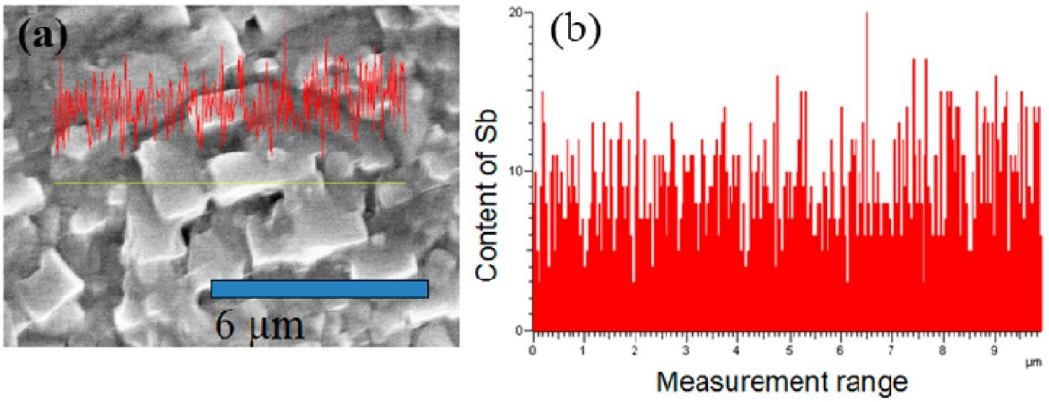

Figure 8. Sb mapping in KNLNS$_x$-BZ ceramics with x = 0.07 analyzed on a line of ~10 μm length.

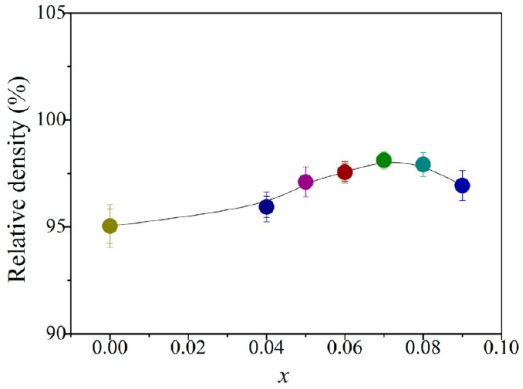

Figure 9. Relative density of of KNLNS$_x$-BZ ceramics as a function of Sb content.

with R-O or O-T phase boundaries,[3−18,20−26,28−34] is comparable to the textured KNN-based ceramic,[3] and is also larger than those with the R-T phase boundary,[19,27] as shown in Table 2.

To investigate the effect of the poling electric field on the d_{33} of the KNLNS$_x$-BZ ceramics, we characterize the poling electric field dependence of the d_{33}, as shown in Figure 13. It is difficult to pole the ceramic with x = 0 fully in the applied electric field range, while the d_{33} of the KNLNS$_x$-BZ ceramics with $x \geq 0.04$ becomes easily saturated under the applied electric field. In this work, the E_{on} is defined as a saturated electric field, depending on their compositions. It is found that the ceramic with x = 0.07 has a lowest E_{on}, showing that the R-T phase boundary facilitates the rotation of the domains during poling.[1,2]

Table 2. Piezoelectric Properties of KNN-Based Ceramics with R-T Phase Boundary

composition	phase boundary	d_{33} (pC/N)	k_p	T_C (°C)	ref
KNN-$BaZrO_3$−$LiSbO_3$	R-T	344	0.33	180	Liang[27]
KNNS-$LiTaO_3$−$BaZrO_3$	R-T	365	0.45	180	Zuo[19]
KNLNS-BZ	R-T	425	0.50	197	This work

In this work, the KNLNS$_x$-BZ ceramic with x = 0.07 has a giant d_{33} of ~425 pC/N, and the underlying physical mechanism for the enhanced piezoelectric behavior has been given here. First, it is well-known that the R-T phase boundary can improve the piezoelectric properties of the PZT because of the involvement of the more polarization states,[1,2] helping the rotation of the ferroelectric domains. As a result, the R-T phase boundary must be mainly responsible for the enhanced piezoelectric behavior of this work.[48] In addition, the enhancement in $\varepsilon_r P_r$ has a close relationship with the d_{33}, i.e., $d_{33} \sim \varepsilon_r P_r$.[27,49] In this work, we plotted $\varepsilon_r P_r$ vs Sb content of all the ceramics, as shown in Figure 14. As shown in this figure, a maximum $\varepsilon_r P_r$ has been observed in the ceramic with x = 0.07. By considering the d_{33} in Figure 12, the close relationship

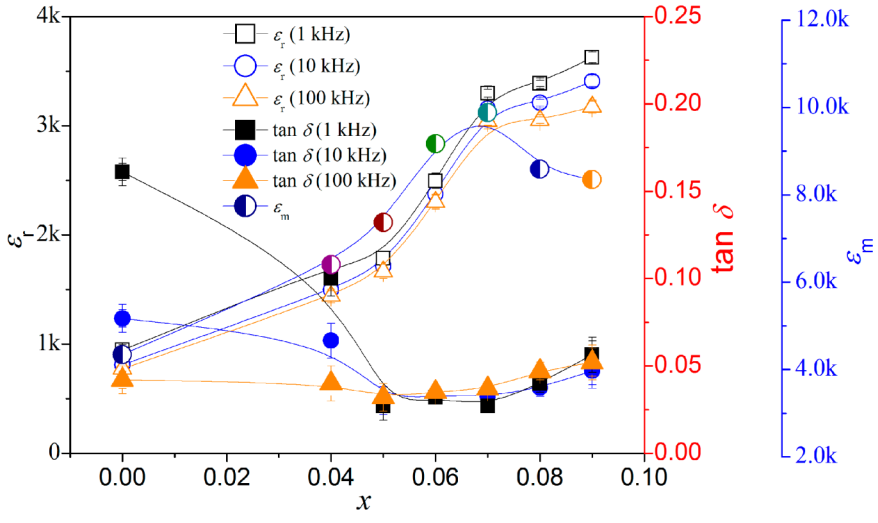

Figure 10. Dielectric properties of of KNLNS$_x$-BZ ceramics at 1−100 kHz.

dx.doi.org/10.1021/am402548x | ACS Appl. Mater. Interfaces 2013, 5, 7718−7725

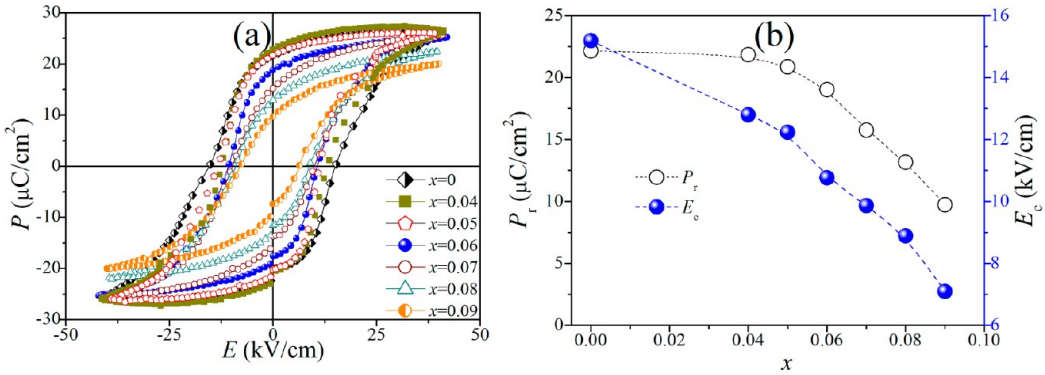

Figure 11. (a) P–E loops and (b) P_r and E_c vs x of KNLNS$_x$-BZ ceramics.

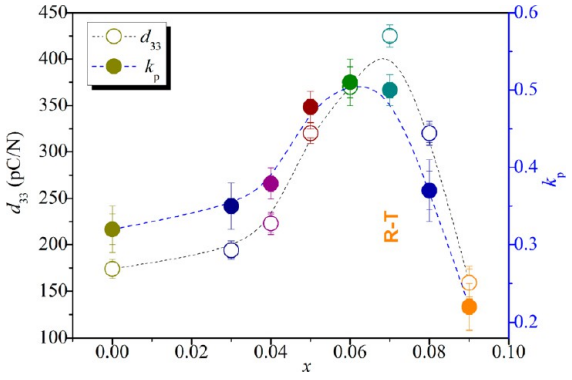

Figure 12. d_{33} and k_p of of KNLNS$_x$-BZ ceramics as a function of Sb content.

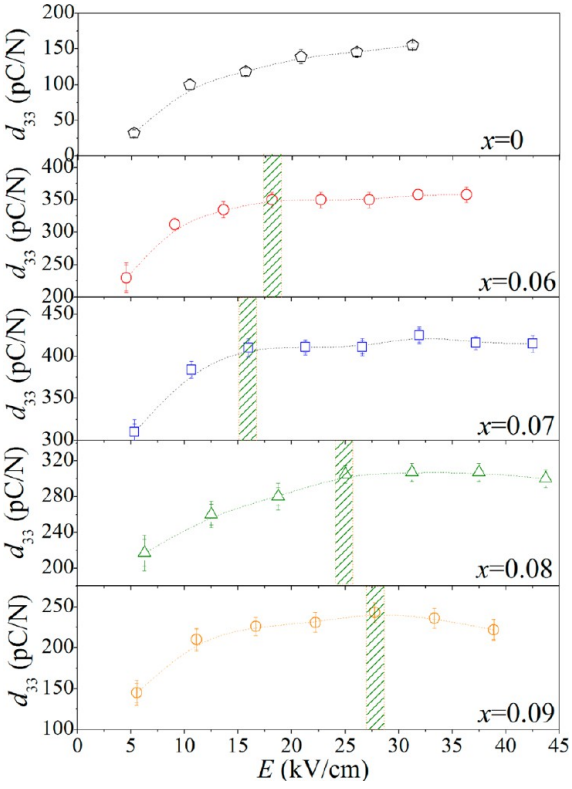

Figure 13. Poling electric field dependence of the d_{33} of KNLNS$_x$-BZ ceramics.

between d_{33} and $\varepsilon_r P_r$ is well established, that is, a higher $\varepsilon_r P_r$ results in a larger d_{33}. In addition, the density could be

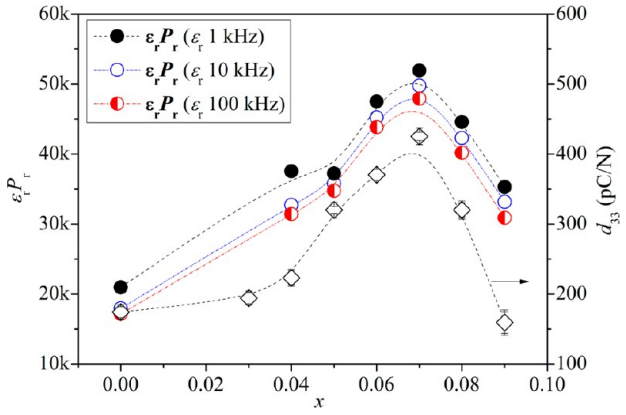

Figure 14. $\varepsilon_r P_r$ vs Sb content of KNLNS$_x$-BZ ceramics.

attributed to the improvement in d_{33} of KNN ceramics,[50] and therefore, the improved density of this work is also partly responsible for the enhanced d_{33}.

4. CONCLUSION

$0.96(K_{0.5}Na_{0.5})_{0.95}Li_{0.05}Nb_{1-x}Sb_xO_3-0.04BaZrO_3$ lead-free ceramics with a giant d_{33} of ~425 pC/N have been prepared by the normal sintering. The rhombohedral–tetragonal phase boundary has been identified in the composition range of $0.04 \leq x \leq 0.07$, as confirmed by the XRD patterns and the temperature -dependent dielectric behavior. In addition, the phase diagram clearly illuminates the phase evolution of the ceramics. Such a ceramic with $x = 0.07$ has largest d_{33} of ~425 pC/N among these reported KNN-based materials, and the formation of the R-T phase coexistence and the enhancement in ε_r and P_r could be largely attributed to the enhanced piezoelectric behavior, showing the most promising lead-free piezoelectrics for the practical applications.

AUTHOR INFORMATION

Corresponding Author

*E-mail: msewujg@scu.edu.cn or wujiagang0208@163.com.

Notes

The authors declare no competing financial interest.

ACKNOWLEDGMENTS

The authors gratefully acknowledge the supports of the National Science Foundation of China (NSFC 51102173 and 51272164), the introduction of talent start funds of Sichuan University (2082204144033), and the Fundamental Research Funds for the Central Universities (2012SCU04A01).

REFERENCES

(1) Jaffe, B.; Roth, R. S.; Marzullo, S. *J. Res. Natl. Bur. Stand.* **1955**, *55*, 239−242.
(2) Jaffe, B.; Cook, W. R.; Jaffe, H. *Piezoelectric Ceramics*; Academic: New York, 1971.
(3) Saito, Y.; Takao, H.; Tani, T.; Nonoyama, T.; Takatori, K.; Homma, T.; Nagaya, T.; Nakamura, M. *Nature* **2004**, *432*, 84−87.
(4) Cross, E. *Nature* **2004**, *432*, 24−25.
(5) Zhang, S. J.; Xia, R.; Shrout, T. R. *J. Appl. Phys.* **2006**, *100*, 104−108.
(6) Zhang, S. J.; Xia, R.; Shrout, T. R. *Appl. Phys. Lett.* **2007**, *91*, 132913.
(7) Rödel, J.; Jo, W.; Seifert, K. T. P.; Anton, E. M.; Granzow, T.; Damjanovic, D. *J. Am. Ceram. Soc.* **2009**, *92*, 1153−1177.
(8) Akdogan, E. K.; Kerman, K.; Abazari, M.; Safari, A. *Appl. Phys. Lett.* **2008**, *92*, 112908.
(9) Wang, K.; Li, J. F. *Adv. Funct. Mater.* **2010**, *20*, 1924−1929.
(10) Guo, Y.; Kakimoto, K.; Ohsato, H. *Appl. Phys. Lett.* **2004**, *85*, 4121−4123.
(11) Malic, B.; Bernard, J.; Holc, J.; Jenko, D.; Kosec, M. *J. Eur. Ceram. Soc.* **2005**, *25*, 2707−2711.
(12) Zuo, R. Z.; Rödel, J.; Chen, R. Z.; Li, L. T. *J. Am. Ceram. Soc.* **2006**, *89*, 2010−2015.
(13) Damjanovic, D. *Appl. Phys. Lett.* **2010**, *97*, 062906.
(14) Matsubara, M.; Kikuta, K.; Hirano, S. *J. Appl. Phys.* **2005**, *97*, 114105.
(15) Malic, B.; Bernard, J.; Holc, J.; Jenko, D.; Kosec, M. *J. Eur. Ceram. Soc.* **2008**, *28*, 1191−1196.
(16) Gao, Y.; Zhang, J.; Qing, Y.; Tan, Y.; Zhang, Z.; Hao, X. *J. Am. Ceram. Soc.* **2011**, *94*, 2968−2973.
(17) Zuo, R. Z.; Fu, J.; Lv, D. Y. *J. Am. Ceram. Soc.* **2009**, *92*, 283−285.
(18) Zuo, R. Z.; Fu, J.; Lv, D. Y.; Liu, Y. *J. Am. Ceram. Soc.* **2010**, *93*, 2783−2787.
(19) Zuo, R. Z.; Fu, J. *J. Am. Ceram. Soc.* **2011**, *94*, 1467−1470.
(20) Zang, G. Z.; Wang, J. F.; Chen, H. C.; Su, W. B.; Wang, C. M.; Qi, P.; Ming, B. Q.; Du, J.; Zheng, L. M.; Zhang, S. J. *Appl. Phys. Lett.* **2006**, *88*, 212908.
(21) Zhang, S. J.; Xia, R.; Shrout, T. R.; Zang, G. Z.; Wang, J. F. *Solid State Commun.* **2007**, *141*, 675−679.
(22) Hao, J. G.; Xu, Z. J.; Chu, R. Q.; Zhang, Y. J.; Li, G. R.; Yin, Q. R. *Phys.B.* **2009**, *404*, 1974−1978.
(23) Guo, X.; Zhu, N.; Xiao, M.; Wu, X. W. *J. Am. Ceram. Soc.* **2007**, *90*, 2467−2471.
(24) Li, H.; Shih, W. Y.; Shih, W. H. *J. Am. Ceram. Soc.* **2007**, *90*, 3070−3072.
(25) Guo, Y. P.; Kakimoto, K.; Ohsato, H. *Mater. Lett.* **2005**, *59*, 241−244.
(26) Hollenstein, E.; Davis, M.; Damjanovic, D.; Setter, N. *Appl. Phys. Lett.* **2005**, *87*, 182905.
(27) Liang, W. F.; Wu, W. J.; Xiao, D. Q.; Zhu, J. G.; Wu, J. G. *J. Mater. Sci.* **2011**, *46*, 6871−6876.
(28) Wu, J. G.; Xiao, D. Q.; Wang, Y. Y.; Zhu, J. G.; Yu, P.; Jiang, Y. H. *J. Appl. Phys.* **2007**, *102*, 114113.
(29) Lin, D.; Kwok, K. W.; Lam, K. H.; Chan, H. L. *J. Appl. Phys.* **2007**, *101*, 074111.
(30) Wu, J. G.; Xiao, D. Q.; Wang, Y. Y.; Zhu, J. G.; Wu, L.; Jiang, Y. H. *Appl. Phys. Lett.* **2007**, *91*, 252907.
(31) Wu, J. G.; Wang, Y. Y.; Xiao, D. Q.; Zhu, J. G.; Pu, Z. H. *Appl. Phys. Lett.* **2007**, *91*, 132914.
(32) Du, J.; Wang, J. F.; Zang, G. Z.; Yi, X. J. *Phys.B.* **2011**, *406*, 4077−4079.
(33) Yoo, J. *Ferroelectrics* **2012**, *437*, 81−87.
(34) Wu, J. G.; Wang, Y. Y.; Xiao, D. Q.; Zhu, J. G.; Yu, P.; Wu, L.; Wu, W. J. *Jpn. J. Appl. Phys.* **2007**, *46*, 7375−7377.
(35) Pan, J. S.; Zhang, X. W.; Chen, K. P. *J. Cryst. Growth* **2005**, *284*, 275−280.
(36) Zhen, Y.; Li, J. F. *J. Am. Ceram. Soc.* **2006**, *89* (12), 3669−3675.
(37) Li, H. D.; Shih, W. Y.; Shih, W. H. *J. Am. Ceram. Soc.* **2007**, *90*, 3070−3072.
(38) Hagh, N. M.; Jadidian, B.; Ashbahian, E.; Safari, A. *IEEE Trans. Ultrason. Ferroelectr.* **2008**, *55*, 214−224.
(39) Kumar, K.; Singh, B. K.; Gupta, M. K.; Sinha, N.; Kumar, B. *Ceram. Int.* **2011**, *37*, 2997−3004.
(40) Egerton, L.; Dillon, D. M. *J. Am. Ceram. Soc.* **1959**, *42*, 438−442.
(41) Ahn, C. W.; Park, C. S.; Choi, C. H.; Nahm, S.; Yoo, M. J.; Lee, H. G.; Priya, S. *J. Am. Ceram. Soc.* **2009**, *92*, 2033−2038.
(42) Hao, J. G.; Xu, Z. J.; Chu, R. Q.; Zhang, Y. J.; Fu, P.; Li, G. R.; Yin, Q. R. *Phys. B* **2009**, *404*, 3391−3396.
(43) Pang, X. M.; Qiu, J. H.; Zhu, K. J.; Cao, Y. *Ceram. Int.* **2012**, *38*, 1249−1254.
(44) Zhang, B. Y.; Wang, X. P.; Cheng, X. J.; Zhu, J. G.; Xiao, D. Q.; Wu, J. G. *J. Alloys Compd.* **2013**, *581*, 446−451.
(45) Huo, S. X.; Yuan, S. L.; Tian, Z. M.; Wang, C. H.; Qiu, Y. *J. Am. Ceram. Soc.* **2012**, *95*, 1383−1387.
(46) Liu, J. S.; Zhang, S. R.; Zeng, H. Z.; Yang, C. T.; Yuan, Y. *Phys. Rev. B.* **2005**, *72*, 172101.
(47) Huang, H.; Sun, C. Q.; Zhang, T. S.; Peter, H. *Phys. Rev. B.* **2001**, *63*, 184112.
(48) Liu, W. F.; Ren, X. B. *Phys. Rev. Lett.* **2009**, *103*, 257602.
(49) Park, S. E.; Shrout, T. R. *IEEE Trans. Ultrason. Ferroelectr.* **1997**, *44*, 1140−1147.
(50) Birol, H.; Damjanovic, D.; Setter, N. *J. Eur. Ceram. Soc.* **2006**, *26*, 861−866.